AIP | Review of Scientific Instruments

High resolution resistive thermometry for micro/nanoscale measurements

S. Sadat, E. Meyhofer, and P. Reddy

Citation: Rev. Sci. Instrum. **83**, 084902 (2012); doi: 10.1063/1.4744963
View online: http://dx.doi.org/10.1063/1.4744963
View Table of Contents: http://rsi.aip.org/resource/1/RSINAK/v83/i8
Published by the AIP Publishing LLC.

High resolution resistive thermometry for micro/nanoscale measurements

S. Sadat,[1] E. Meyhofer,[1,a)] and P. Reddy[1,2,b)]
[1]*Department of Mechanical Engineering, University of Michigan, Ann Arbor, Michigan 48109, USA*
[2]*Department of Materials Science, University of Michigan, Ann Arbor, Michigan 48109, USA*

(Received 16 June 2012; accepted 26 July 2012; published online 24 August 2012)

High resolution thermometry plays an important role in several micro/nanoscale studies. Here, we present a detailed analysis of the resolution of resistance thermometry schemes that employ an electrical sensing current to monitor the temperature-dependent resistance. Specifically, we theoretically and experimentally analyze four different schemes where modulated or unmodulated temperatures in microdevices are measured using modulated or unmodulated sensing currents. Our analysis and experiments suggest that measurement of unmodulated temperatures using a modulated sensing current improves the resolution in comparison to a scenario where an unmodulated sensing current is used. However, depending on the exact measurement conditions, such improvements might be modest as the overall resolution may be limited by random low frequency environmental temperature fluctuations. More importantly, we find that high-resolution thermometry can be achieved in the measurement of modulated temperatures. Specifically, we show that by using appropriate instrumentation and a 10 kΩ platinum resistance thermometer it is possible to measure modulated temperatures (0.5–20 Hz) with a resolution of about 20–100 μK. The advances described here will enable a dramatic improvement in the heat-current resolution of resistive thermometry based microdevices that are used for probing nanoscale phonon and photon transport. © *2012 American Institute of Physics*. [http://dx.doi.org/10.1063/1.4744963]

I. INTRODUCTION

High-resolution thermometry plays a critical role in the function of a variety of microdevices[1–4] including ultra-high resolution calorimeters,[5,6] scanning thermal imaging probes,[7] and suspended microdevices used for probing energy transport at the nanoscale.[1,8,9] As a concrete example, consider the role of thermometry in probing nanoscale heat transport. A majority of nanoscale heat transport studies utilize a microfabricated suspended island with an integrated thermometer that functions as a heat flow calorimeter[5] (Fig. 1). The ultimate heat flow resolution (Q_{Res}) of such a microdevice depends on the thermal conductance between the thermally isolated region and the thermal reservoir (G_{Th}) and the resolution of the thermometer (ΔT_{Res}) and is given by $Q_{Res} = G_{Th} \cdot \Delta T_{Res}$. Therefore, performing high-resolution thermometry is critical for measuring small heat currents.

Resistance thermometry is one of the most widely used approaches to measure temperature changes at the microscale. The popularity of this approach stems from the relative ease with which it can be implemented in comparison to other approaches such as bimaterial cantilever based thermometers that offer high resolution.[3,10,11] Microscale resistance thermometry is typically implemented using a thin film platinum resistance thermometer (PRT), whose electrical resistance increases almost linearly with temperature over a wide range of temperatures.

In this article, we present a detailed analysis of the noise characteristics of resistance thermometers. We analyze the various contributions to noise that limit the resolution of resistance thermometry. Specifically, we analyze the resolution of PRTs in four different scenarios: (1) measurement of an unmodulated temperature using an unmodulated (dc) electrical current, (2) measurement of an unmodulated temperature using a sinusoidally modulated sensing current, (3) measurement of a modulated temperature using an unmodulated sensing current, and (4) measurement of a sinusoidally modulated temperature using a sinusoidal sensing current. Our analysis and experiments identify the limits to resolution in each of these scenarios and provide the information necessary to determine when each of these schemes can be beneficially employed.

II. NOISE SOURCES IN RESISTANCE THERMOMETRY

Resistance thermometry is based on the measurement of the electrical resistance (R) of a temperature-dependent resistive element that is in thermal equilibrium with the object whose temperature (T) is to be measured. To understand the factors that limit the resolution of a resistance thermometer it is instructive to consider the configuration shown in Fig. 2(a). In such a configuration, the resistance ($R(T)$) is monitored by passing a known sensing current (I_s) through it and measuring the resulting potential difference (V) across it. Subsequently, the desired temperature is obtained from the calibrated relationship between electrical resistance and temperature. Although resistors made from copper, gold, platinum, and niobium are used, PRTs are the most popular choice due to their stability in different environments[12] and the almost linear dependence of their resistance on temperature[13] over a broad range of temperatures. The measured temperature dependence of the PRTs is typically tabulated using the Callendar-Van Dusen equation[13] or other

a)Electronic mail: meyhofer@umich.edu.
b)Electronic mail: pramodr@umich.edu.

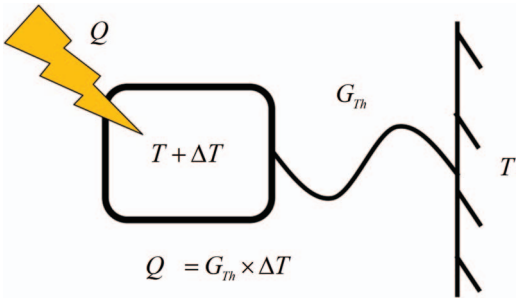

FIG. 1. Principle of heat flow calorimetry. The sensing stage is isolated from the thermal reservoir by a finite thermal conductance (G_{Th}). The magnitude of the heat current is quantified by measuring the temperature difference ΔT.

polynomial relations.[13] Alternatively, it is also expressed in a closed form using the Bloch-Grüneison formula.[14]

In order to measure small temperature changes it is convenient to define a term called the temperature coefficient of resistance (TCR), which is conventionally denoted by the symbol α. At any temperature, TCR is defined by $\alpha(T) = (dR/dT)/R(T)$. The change in the temperature of the resistor (ΔT) can then be directly obtained from $\Delta T = \Delta V_{RTI}/[I_s R(T)\alpha]$, where ΔV_{RTI} is obtained by dividing the voltage change (ΔV_{Out}) at the output of the amplifier by the amplifier gain G_1. We note that the voltage changes are measured in a bandwidth Δf. This equation suggests that the noise equivalent temperature (NET) that represents the temperature resolution (ΔT_{Res}) of a resistance based thermometer is given by

$$\mathrm{NET} = \Delta T_{Res} = \frac{\Delta V_{Noise,RTI}}{[I_s R(T)\alpha]}, \tag{1}$$

where $\Delta V_{Noise,RTI}$ is the root mean square (RMS) value of the voltage noise (measured relative to the inputs) in the measurement bandwidth Δf. This suggests that, if the heating power is not a constraint, employing large sensing currents (I_s) or choosing a PRT with a large R can enable very high resolution measurements. However, in certain scenarios large sensing currents result in self-heating effects that are detrimental to the measurement as well as device stability, in which case it is necessary to choose a resistance thermometer with a larger value of α to obtain a higher resolution. Specifically, the impact of self-heating on the temperature rise depends on the thermal conductance (G_{th}) between the thermally isolated region and the thermal reservoir (Fig. 1) and must be taken into account while choosing the sensing current. Further, we note that in microdevices it is not always feasible to increase the resistance to large values due to constraints on the maximum possible footprint of the resistor. Hence, to maximize temperature resolution it is important to understand the limitations imposed by various noise sources on $\Delta V_{Noise,\ RTI}$.

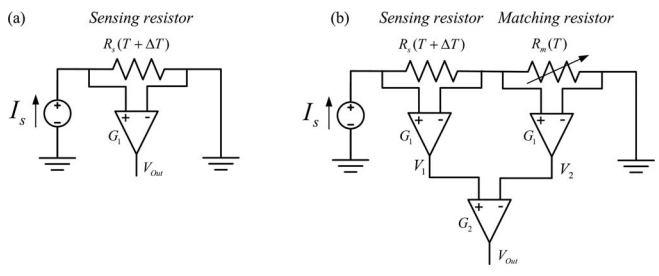

FIG. 2. Principle of resistive thermometry. (a) The electrical resistance is monitored by passing a known current and measuring the voltage drop across the resistor. The temperature of the object of interest is obtained by calibrating the relationship between resistance and temperature. (b) Differential measurement scheme for isolating the signal of interest by rejecting the common mode voltage. The effect of drift in the environmental temperature is also attenuated by the differential scheme.

The noise in the voltage signal has multiple components, which could be broadly categorized as *intrinsic* (Johnson and shot) and *non-intrinsic* noise (e.g., *1/f* noise, amplifier noise, etc.). To perform high-resolution thermometry, it is necessary to quantify the contribution of these noise sources. We now provide a brief description of the power spectral density (*PSD*) of various noise sources.

Johnson noise arises due to spontaneous thermal fluctuations of charge in a resistor. For frequencies below 1 MHz and temperatures above 25 K the *PSD* of Johnson noise is well approximated by[15] $PSD_{V,Johnson}[\mathrm{V^2/Hz}] = 4k_BTR$, where k_B is Boltzmann's constant, T is the equilibrium temperature of the reservoir, and R is the resistance (the units of the *PSD* are shown in the square brackets). Shot noise arises from the granular nature of charge, which manifests itself as fluctuations in the sensing current. The power spectral density of shot noise is well approximated by[15] $PSD_{I,\ Shot}[\mathrm{Amp^2/Hz}] = 2qI_s$, where q is the charge of a proton, and I_s is the magnitude of the sensing current supplied through the resistor (Fig. 2(a)). In addition to this noise, the sensing current may also have additional noise contributions due to non-idealities (NI) in the current source, which can be quantified by directly measuring the *PSD* of the current source ($PSD_{I,\ NI}$)[$\mathrm{Amp^2/Hz}$]. The low frequency noise arising from ambient temperature changes and structural changes in the electronic components comprising the measurement setup is collectively called 1/*f* noise. Since an *a priori* estimation of the power spectral density of 1/*f* noise ($PSD_{1/f}$ [$\mathrm{V^2/Hz}$]) is usually difficult it is characterized experimentally.

Amplifier noise is the cumulative effect of non-idealities in the amplifier components, which manifest as voltage noise at the output of an amplifier. Amplifier noise has two independent components: the relative-to-input voltage noise (RTI) and input current (IC) noise.[16] The power spectral density of the RTI noise ($PSD_{V,\ RTI}$ [$\mathrm{V^2/Hz}$]) depends on both the gain of the amplifier and frequency. The IC noise of the amplifier is a frequency dependent noise at the input of the amplifier due to a finite current flow into the amplifier and is represented by $PSD_{I,\ IC}$ [$\mathrm{Amp^2/Hz}$]. The contribution of each of these sources depends on the detailed design of the amplifier/instrument under consideration and is usually characterized experimentally.

The total power spectral density of noise ($PSD_{Noise,\ RTI}$) relative to the input of the amplifier shown in Fig. 2(a) can be obtained from (assuming that all noise is uncorrelated)[17]

$$PSD_{Noise,RTI} = [(PSD_{V,Johnson}) + (PSD_{I,Shot} + PSD_{I,NI} + PSD_{I,IC})R^2 + PSD_{V,RTI} + PSD_{V,1/f}]. \tag{2}$$

The RMS value of the voltage noise relative to the inputs ($\Delta V_{Noise,\,RTI}$), in the bandwidth of interest (f_0, $f_0 + \Delta f$), can then be obtained from

$$\Delta V_{Noise,\,RTI} = \left[\int_{f_0}^{f_0+\Delta f} PSD_{Noise,RTI}(f)df\right]^{1/2}. \quad (3)$$

Using this expression and Eq. (1) the NET of a resistance thermometer can be estimated.

A. Differential scheme for measuring small temperature changes

Measurement of small temperature changes using the scheme shown in Fig. 2(a), especially when the temperature changes are unmodulated, is limited by fluctuations in ambient temperature, which leads to spurious measurements. Furthermore, since the change in the voltage signal resulting from the small temperature change, ΔT, is relatively small, an instrument with a large dynamic range is required.

The problems associated with temperature drift and the required dynamic range can be addressed by adopting the differential scheme shown in Fig. 2(b), which in fact represents one half of a Wheatstone bridge network. Full bridge configurations are frequently employed in related measurement applications (with some relatively small advantages and disadvantages), but since it is generally not feasible to fabricate multiple sensing resistors into micro- and nanoscale device structures of interest, we focus in this work on the configuration shown in Fig. 2(b). Overall, this configuration offers lower noise given the smaller overall source resistance. We note that the analysis for a full bridge is nearly identical.

In the configuration shown in Fig. 2(b), a second "matching" resistor whose resistance and TCR values are chosen to be "very" close to that of the "sensing" resistor is incorporated. The sensing resistor experiences a temperature change ΔT whereas the matching resistor does not. The voltage outputs across the sensing and matching resistors are measured using two instrumentation amplifiers (first stage) and subsequently subtracted from each other using another instrumentation amplifier (second stage). This scheme accomplishes two purposes: (1) the common mode voltage across the two resistors is eliminated (discussed in more detail below), enabling the isolation of the signal arising from the temperature change ΔT, and (2) if the matching resistor is in excellent contact with the same thermal reservoir that the sensing resistor is coupled to, then the effects of environmental temperature drift can be significantly attenuated as both the resistors sense similar (although not identical) temperature drifts. As explained later, the use of such a thermally coupled matching resistor is critical for the measurement of unmodulated temperature changes—in fact, this idea is the key to the improvements reported by Wingert *et al.*[2,8] in their recent work on probing heat transfer in nanostructures with high resolution.

TABLE I. Different schemes for resistance thermometry. The temperature is either modulated at a frequency (f_T) or is not modulated. Similarly, the electrical current for sensing resistance changes is either modulated at a frequency (f_s) or is not modulated.

Scheme	Temperature change	Sensing current	Sensing frequency
1	Unmodulated, $f_T = 0$	Unmodulated, $f_s = 0$	0
2	Unmodulated, $f_T = 0$	Modulated, f_s	f_s
3	Modulated, f_T	Unmodulated, $f_s = 0$	f_T
4	Modulated, f_T	Modulated, f_s	$f_s - f_T, f_s + f_T$

III. SCHEMES TO MEASURE SINUSOIDALLY MODULATED AND UNMODULATED TEMPERATURE CHANGES

In this section we present a detailed discussion of different resistance thermometry schemes (Table I). Specifically, we will examine the advantages and disadvantages of the four possible schemes involving the measurement of unmodulated or sinusoidally modulated temperatures using unmodulated or sinusoidally modulated sensing currents. Further, we also develop expressions to estimate the resolution achievable using each of these schemes.

A. Scheme 1: Measurement of unmodulated temperature changes (ΔT) using unmodulated sensing current (I_s)

In this *scenario*, the output signal of the second stage amplifier (Fig. 2(b)) is given by

$$V_{Out} = \underbrace{G_1 G_2 [I_s R \alpha \Delta T]}_{V_{Signal}} + \Delta V_{Noise}, \quad (4)$$

where G_2 is the gain of the stage 2 amplifier (Fig. 2(b)). Equation (4) shows that the signal of interest is at $f = 0$ Hz as both the sensing current and the temperature change are unmodulated. The voltage noise (ΔV_{Noise}) can be obtained by estimating the power spectral density of the noise at the output of the second stage amplifier ($PSD_{Amp\ Total}$):

$$\begin{aligned} PSD_{Amp\,Total}(f) &= [2[PSD_{noise,RTI}(f) - PSD_{I,NI}(f)R^2]G_1^2 \\ &\quad + PSD_{V,RTI,Amp2}(f) + PSD_{V,1/f,Amp2}(f)]G_2^2, \end{aligned} \quad (5)$$

where $PSD_{Noise,\,RTI}$ is defined by Eq. (2), $PSD_{I,NI}$ is the noise due to the non-ideal behavior of the current source, $PSD_{V,\,RTI,\,Amp2}$ refers to the relative to input noise of the stage 2 amplifier, and $PSD_{V,\,1/f,\,Amp2}$ refers to the $1/f$ noise of the stage 2 amplifier (Fig. 2(b)). We note that in Eq. (5), $PSD_{I,NI}(f)R^2$ is subtracted from the $PSD_{Noise,\,RTI}$ because the effect of non-ideality of the current source is eliminated in a differential scheme. The power spectral density of the noise is usually reported relative to input as ($PSD_{Amp\ Total,\,RTI}$):

$$PSD_{Amp\,Total,RTI}(f) = \frac{PSD_{Amp\,Total}(f)}{[G_1 G_2]^2}. \quad (6)$$

Therefore, the mean square voltage noise at $f = 0$ Hz (the frequency of interest here), relative to the inputs, can now be estimated as

$$\Delta V^2_{Amp\,Total,RTI,S1} = \int_0^{\Delta f} PSD_{Amp\,Total,RTI}(f)df, \tag{7}$$

where Δf is the bandwidth of the measurement. We note that in this scheme, $\Delta V_{Amp\ Total,\ RTI,\ S1}$ is large because $PSD_{Amp\ Total,\ RTI}(f = 0\ \text{Hz})$ is expected to have large contributions from $1/f$ noise.

In addition to the voltage noise described above, it is also necessary to consider the effect of the relative drift in the temperatures of the sensing and matching resistors. To elaborate, let the temperature of the sensing resistor, at time t, be $T_1(t) + \Delta T$, where ΔT is the unmodulated temperature to be measured, whereas the temperature of the matching resistor is $T_2(t)$. Ideally, $T_2(t) - T_1(t)$ should be equal to zero, in which case the temperature difference between the matching and sensing resistors would be equal to ΔT. However, due to temperature drift the actual temperature difference (ΔT (*non-ideal*)) is given by

$$\begin{aligned}\Delta T(non\,ideal) &= \Delta T(ideal) + [T_1(t) - T_2(t)] \\ &= \Delta T(ideal) + \Delta T_{Drift}(t).\end{aligned} \tag{8}$$

The effect of temperature related drift can be quantified from a knowledge of the power spectral density of ΔT_{Drift}, $PSD_{\Delta T,\ Drift}$ [K^2/Hz]. The mean square voltage noise, relative to the input, associated with temperature drift $\Delta V_{Temperature\ Drift,\ RTI}$ can then be expressed as

$$\begin{aligned}&\Delta V^2_{Temperature\,Drift,\,RTI,\,S1}(f = 0Hz) \\ &= (I_s R\alpha)^2 \int_0^{\Delta f} PSD_{\Delta T,\,Drift}(f)df.\end{aligned} \tag{9}$$

In practice this effect is frequently large because the relative temperature drift at low frequencies can be substantial (quantified in Sec. V). Therefore, the noise equivalent temperature for scheme 1 ($\text{NET}_{\text{Scheme 1}}$) can be expressed as

$$\text{NET}_{\text{Scheme 1}} = \frac{\left[\Delta V^2_{Amp\,Total,\,RTI,\,S1} + \Delta V^2_{Temperature\,Drift,\,RTI,\,S1}\right]^{1/2}}{I_s R\alpha}. \tag{10}$$

This equation suggests that $\text{NET}_{\text{Scheme1}}$ will be limited by $\Delta V^2_{Amp\,Total,\,RTI,\,S1}(f = 0\,\text{Hz})$ and/or $\Delta V^2_{Temperature\,Drift,\,RTI,\,S1}(f = 0\,\text{Hz})$, depending on their relative magnitude (quantified later in Sec. V).

B. Scheme 2: Measurement of unmodulated temperature changes (ΔT) using modulated sensing current (I_s)

The large contribution of low frequency noise to the NET in scheme 1 can be significantly reduced by using a modulated sensing current ($I_s \sin(2\pi f_s t)$). The output voltage signal in this scheme is given by

$$V_{Out} = \underbrace{G_1 G_2[I_s \sin(2\pi f_s t) R\alpha \Delta T]}_{V_{Signal}} + \Delta V_{Noise}, \tag{11}$$

where I_s and f_s are the amplitude and frequency of the sensing current, respectively. Equation (11) shows that the signal of interest is now modulated at frequency f_s, which can usually be chosen to be sufficiently large to effectively reduce voltage noise. This can be best understood by noting that the mean square voltage noise is given by

$$\begin{aligned}&\Delta V^2_{Amp\,Total,\,RTI,\,S2}(f = f_s\text{Hz}) \\ &= \int_{f_s - \Delta f/2}^{f_s + \Delta f/2} PSD_{Amp\,Total,\,RTI}(f)df.\end{aligned} \tag{12}$$

Therefore, if f_s is large (say >100 Hz) the voltage noise will be substantially smaller as compared to that at lower frequencies where the contribution of the $1/f$ noise is large. With a modulated sensing current ($I_s \sin(2\pi f_s t)$), the mean square voltage noise associated with the temperature drift, at the frequency of interest (f_s), is given by (see Appendix for more details)

$$\begin{aligned}&\Delta V^2_{Temperature\,Drift,\,RTI,\,S2}(f = f_s\,\text{Hz}) \\ &\sim \frac{(I_s R\alpha)^2}{2} \int_0^{\Delta f/2} PSD_{\Delta T,\,Drift}(f = 0\,\text{Hz})df.\end{aligned} \tag{13}$$

The noise equivalent temperature for scheme 2 ($\text{NET}_{\text{Scheme 2}}$) is therefore given by

$$\text{NET}_{\text{Scheme 2}} = \frac{\left[\Delta V^2_{Amp\,Total,\,RTI,\,S2} + \Delta V^2_{Temperature\,Drift,\,RTI,\,S2}\right]^{1/2}}{I_s R\alpha}. \tag{14}$$

Equations (13) and (14) suggest that by using a modulated sensing current the effect of $1/f$ voltage noise can be substantially reduced. However, the effect of temperature drift between the *matching* and *sensing* resistors can still be large because $PSD_{\Delta T,\,Drift}(f = 0\ \text{Hz})$ is typically large at low frequencies (quantified in Sec. V). Thus, minimizing $PSD_{\Delta T,\,Drift}$ at low frequencies is critical for further reducing the NET.

C. Scheme 3: Measurement of modulated temperature changes (ΔT) using an unmodulated sensing current (I_s)

We now consider a measurement scheme where the temperature can be modulated at a known frequency f_T. Measurement of modulated temperatures is critical for performing high-resolution calorimetry[5] and photothermal measurements.[11] In order to measure modulated temperature oscillations, we consider the situation where the sensing current (I_s) is not modulated, i.e., $f_s = 0$ Hz. In the scheme shown in Fig. 2(b), only the sensing resistor experiences periodic temperature modulations ($\Delta T \sin(2\pi f_T t)$) which results in a

voltage signal at the output of the second amplifier given by

$$V_{Out} = \underbrace{G_1 G_2 [I_s R\alpha \Delta T \sin(2\pi f_T t)]}_{V_{Signal}} + \Delta V_{Noise}, \tag{15}$$

where the signal of interest is at $f = f_T$ Hz. The mean square noise voltage in this scheme can be obtained from

$$\Delta V^2_{Amp\,Total,\,RTI,\,S3}(f = f_T \text{Hz}) = \int_{f_T - \Delta f/2}^{f_T + \Delta f/2} PSD_{Amp\,Total,\,RTI}(f) df. \tag{16}$$

If the frequency of the temperature modulation f_T can be chosen to be relatively large (>100 Hz) the *PSD* of the voltage noise in Eq. (16) can be small relative to the $1/f$ noise. Further, in this scheme the voltage noise associated with temperature drift can also be minimized. To elaborate, the RMS temperature fluctuation ($\Delta T_{Drift,\,RMS}$) that would be measured in a small band of frequencies $f = f_T - \Delta f/2$ to $f = f_T + \Delta f/2$ Hz is given by

$$\Delta T_{Drift,RMS} = \left[\int_{f_T - \Delta f/2}^{f_T + \Delta f/2} PSD_{\Delta T,\,Drift}(f) df \right]^{1/2}. \tag{17}$$

This temperature fluctuation is substantially smaller than that in schemes 1 and 2 as the $PSD_{\Delta T,\,Drift}$ is significantly smaller in the frequency range of interest ($f_T - \Delta f/2$, $f_T + \Delta f/2$). The mean square voltage noise associated with temperature drift, relative to the inputs, in a small band of frequencies ($f_T - \Delta f/2, f_T + \Delta f/2$) is given by

$$\Delta V^2_{Temperature\,Drift,\,RTI,\,S3}(f = f_T \text{Hz}) = (I_s R\alpha)^2 \int_{f_T - \Delta f/2}^{f_T + \Delta f/2} PSD_{\Delta T,\,Drift}(f) df, \tag{18}$$

and the noise equivalent temperature for scheme 3 ($\text{NET}_{\text{Scheme 3}}$) is given by

$$\text{NET}_{\text{Scheme 3}} = \frac{\left[\Delta V^2_{Amp\,Total,\,RTI,\,S3} + \Delta V^2_{Temperature\,Drift,\,RTI,\,S3}\right]^{1/2}}{I_s R\alpha}. \tag{19}$$

Equation (19) suggests that the NET of scheme 3 can be very small if the temperature is modulated at high enough frequencies. However, in certain microdevices, e.g., those used in nanoscale heat transfer studies,[1,5] it is not possible to modulate the temperature at relatively large frequencies, as the suspended devices have thermal cutoff frequencies in the range of 1–10 Hz. The next scheme shows that low NETs can be achieved even in such scenarios by employing a modulated sensing current.

D. Scheme 4: Measurement of modulated temperature changes (ΔT) using a modulated sensing current (I_s)

We now consider the measurement of modulated temperature changes using a modulated sensing current. In this scheme, the voltage signal at the output of the second amplifier is given by

$$V_{Out} = \underbrace{G_1 G_2 [I_s \sin(2\pi f_s t) R\alpha \Delta T \sin(2\pi f_T t)]}_{V_{Signal}} + \Delta V_{Noise}, \tag{20}$$

where I_s is the amplitude of the sensing current and f_T is the frequency of temperature modulation. The voltage signal of interest can now be expressed as

$$V_{Signal} = \frac{G_1 G_2 I_s R\alpha \Delta T}{2} [\cos(2\pi (f_s - f_T)t) - \cos(2\pi (f_s + f_T)t)], \tag{21}$$

which shows that the voltage signal has contributions at two frequencies, $f_s - f_T$ and $f_s + f_T$, both of which can be chosen to be sufficiently large by choosing the sensing frequency f_s to be large even though the temperature modulation frequency f_T may be small.

In order to obtain the desired signal it is necessary to extract the signal components in the frequency bands centered at $(f_s - f_T)$ and $(f_s + f_T)$ in a width Δf. The mean square voltage noise corresponding to measurements in these bands of frequencies is given by

$$\Delta V^2_{Amp\,Total,\,RTI,\,S3} = \int_{f_s - f_T - \Delta f/2}^{f_s - f_T + \Delta f/2} PSD_{Amp\,Total,\,RTI}(f) df + \int_{f_s + f_T - \Delta f/2}^{f_s + f_T + \Delta f/2} PSD_{Amp\,Total,\,RTI}(f) df. \tag{22}$$

Further, the overall noise also has contributions from two frequency windows—instead of one in scheme 3. This does not necessarily increase the total noise as the frequency window can be chosen to be centered at large frequencies, even though the modulation frequency f_T is small. The contribution to the voltage noise from relative temperature drift between the *sensing* and *matching* resistance can be estimated from (see Appendix)

$$\Delta V^2_{Temperature\,Drift,\,Total,\,RTI,\,S4} \sim \frac{(I_s R\alpha)^2}{2} \int_{f_T - \Delta f/2}^{f_T + \Delta f/2} PSD_{\Delta T,\,Drift}(f) df. \tag{23}$$

This suggests that the noise equivalent temperature for scheme 4 can be expressed as

$$\text{NET}_{\text{Scheme 4}} = \frac{\left[\Delta V^2_{Amp\,Total\,RTI,\,S4} + \Delta V^2_{Temperature\,Drift,\,RTI,\,S4}\right]^{1/2}}{I_s R\alpha}. \tag{24}$$

The discussion presented above shows that it is beneficial to use scheme 4 when measuring temperatures that are sinusoidally modulated at low frequencies.

E. Summary and comparison of the four measurement schemes

The detailed discussion presented above lays out the limitations and requirements for achieving high-resolution resistive thermometry. The resolution of resistive thermometry is improved significantly by (1) employing a matching resistor which helps in isolating the signal of interest and rejecting the common mode noise originating from both environmental thermal drift and noise in the sensing current, (2) adopting a modulation scheme that enables measurements at frequencies where the power spectral density of noise is small, and (3) choosing a large sensing current as well as a PRT with a large electrical resistance: parameters which cannot be increased to arbitrarily large values in most micro and nanoscale applications due to self-heating effects and limitation of the device foot print.

It was shown that the resolution of resistive thermometry in scheme 1, measurement of unmodulated temperatures using an unmodulated sensing current, is relatively poor as the large $1/f$ noise (from both voltage noise and temperature drift) results in a large noise signal. The limitations of scheme 1 are partly eliminated in scheme 2 where unmodulated temperatures are measured using modulated sensing currents. In this scheme, the NET is significantly improved as the measurements are made at a relatively high frequency where the contribution of $1/f$ voltage noise is negligible. However, this scheme is still susceptible to noise arising from low-frequency ambient temperature drift limiting the resolution. The noise associated with ambient temperature drift is eliminated if the temperature to be detected is modulated at a relatively high frequency. Specifically, our discussion highlighted the fact that modulated temperatures can be measured using unmodulated electrical current at high resolution (scheme 3). However, if the modulation frequency of the temperature is low, scheme 3 is affected by electrical $1/f$ noise. In order to overcome this challenge, we described a scenario (scheme 4) where a modulated sensing current can be used to detect low frequency temperature modulations. Such a scheme enables measurement at high frequencies attenuating the effect of both $1/f$ noise and temperature drift. However, in implementing such a scheme one has to contend with noise in two spectral windows as the signal is split into two sidebands.

IV. APPROACH FOR EXPERIMENTAL CHARACTERIZATION OF THE NET OF TEMPERATURE MEASUREMENT SCHEMES

In order to experimentally test the NET of the schemes described above it is desirable to fabricate devices that have both an electrical heater and an electrical resistance thermometer in excellent thermal contact with each other. In such a device, the electrical heater can be used for generating temperature changes, while the thermometer can be used to measure the temperature oscillations.

We accomplished this goal by microfabricating devices with an integrated heater and thermometer (Fig. 3). The device, fabricated on a glass substrate, features a 8000 μm long, 20 μm wide, and 100 nm thick Au electrical heater line which

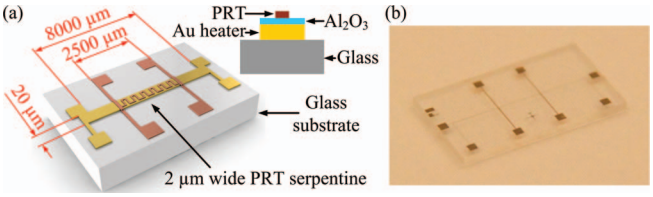

FIG. 3. Microdevice used in this work. (a) Schematic diagram of the test device (not drawn to scale). A micro-heater line (Au heater) patterned on a glass substrate is used to generate temperature modulations. The top PRT is patterned on top of the micro-heater line and separated by a thin Al_2O_3 layer (see cross section) to electrically isolate it from the heater while maintaining it in excellent thermal contact with the heater. Note that the Al_2O_3 layer is not shown in the schematic in order to facilitate a clear view of the heater line. (b) Optical image of the microfabricated test device.

is patterned in a four probe configuration using a lift-off process. Further, a 40 nm thick aluminum oxide (Al_2O_3) film is deposited using atomic layer deposition on the heater line. Finally, a serpentine shaped platinum thin film (see Fig. 3), which is $\sim$2 μm wide and $\sim$35 nm thick and shaped into a four-probe pattern, is deposited on the Al_2O_3 film using a lift-off process. We note that the thin Al_2O_3 film serves to electrically isolate the Au and Pt lines, from each other, while maintaining them in excellent thermal contact. We choose the length of the serpentine line such that the resultant electrical resistance of the PRT is $\sim$10 KΩ. This choice represents a compromise between high temperature resolution and the feasibility of integrating PRTs with a resistance of 1–10 KΩ into microdevices, including suspended devices used in nanoscale heat transport studies.[1] Thus the improvements described in this work can be readily utilized for enhancing the resolution of thermometry used in nanoscale heat transfer studies.

The strategy adopted in this work to characterize the NET of the four schemes is conceptually simple. The microfabricated device is placed in a cryostat (in a vacuum of $\sim 10^{-3}$ torr) and an electrical current (modulated or unmodulated) is supplied to the heater. When a sinusoidal electrical current with a frequency f_H is applied to the heater line it results in temperature oscillations of the heater line at $2f_H = f_T$. The serpentine PRT sensor fluctuates at exactly the same temperature as it is in excellent thermal contact with the heating line through a thermally highly conductive 40 nm thick Al_2O_3 layer (demonstrated experimentally as described later). This can be understood by noting that the thermal coupling between the PRT line and the external environment, through radiation and by conduction through the air molecules, is negligible in comparison with the thermal coupling with the heater line. We now describe in detail our experimental approach.

The first step in characterizing the microfabricated heater and the PRT is to determine the value of the TCR of the Au (heater) and Pt (thermometer) thin films. We measured the TCR by systematically varying the temperature of the cryostat from 80 K to 320 K while monitoring the electrical resistance of the heater and the PRT in a four probe configuration. To elaborate, a sinusoidal current of amplitude $I_{AC} = 10$ μA and frequency $f_s = 100$ Hz was passed through the PRT and the amplitude of the resultant voltage oscillations at 100 Hz (V_{100Hz}), across the serpentine region, was measured using a lock-in amplifier (SR830, Stanford Research

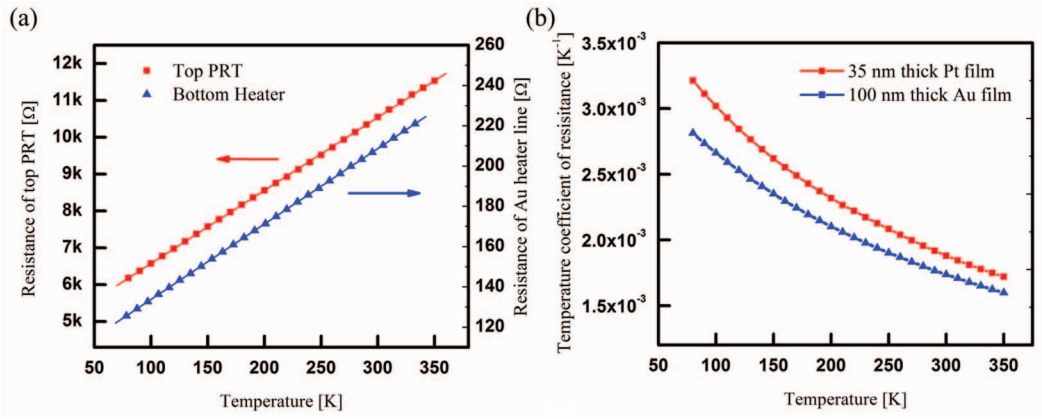

FIG. 4. Characterization of the temperature dependence of resistance. (a) The measured resistance vs. temperature for the PRT and heater lines: red arrow points to the resistance of the PRT whereas the blue arrow points to the resistance of the heater. (b) The obtained TCR values for the 35 nm thick PRT (Pt film) and 100 nm thick heater (Au film) line.

Systems) to obtain the resistance ($R = V_{100Hz}/I_{AC}$). A similar approach was used to measure the temperature dependent resistance of the heater line. Figure 4(a) shows the measured resistance vs. temperature from which the temperature dependent TCRs were calculated (Fig. 4(b)). The measured TCR values are in good agreement with published data for the TCR of Au and Pt thin films of comparable thickness.[1,2]

To show that the heater and thermometer are in excellent thermal contact and experience identical temperature changes, we adopt the configuration shown in Fig. 5. When a sinusoidal heating current $I(t) = I_H \sin(2\pi f_H t)$ generated using a commercially available current source (Keithley-6221) is supplied to the heater its temperature oscillates sinusoidally at a frequency $2f_H$ due to joule heating (f_H was set to 20 Hz in this experiment). Further, the voltage across the probe electrodes (labeled 3 and 4 in Fig. 5) also has a component at $3f_H$, which results from the interaction of the sinusoidal sensing current at f_H and the PRT whose temperature is oscillating sinusoidally at $2f_H$. The RMS value of the sinusoidal temperature oscillation at $2f_H$ (ΔT_{2f_H}) can be related to the RMS value of voltage oscillation at $3f_H$ (V_{3f_H}) by $\Delta T_{2f_H} = 2V_{3f_H}/(I_H R\alpha)$.

In addition to the signal at $3f_H$, the voltage signal across the probe electrodes also has a large component at frequency f_H. In order to extract the voltage component of interest at $3f_H$, we placed a bulk potentiometer (see Fig. 5(a)) in series with the bottom heater. Since the bulk potentiometer has a large thermal mass its amplitude of temperature oscillation at $2f_H$ is negligible. Thus the voltage drop across the potentiometer primarily has a component at the frequency f_H, which can be made identical to the component across the heater by appropriately tuning the resistance of the potentiometer. The voltage output across the bottom heater and that across the potentiometer are first measured using two precision instrumentation amplifiers (A1, A2, Analog Devices - AD524), each of which is chosen to have a gain of

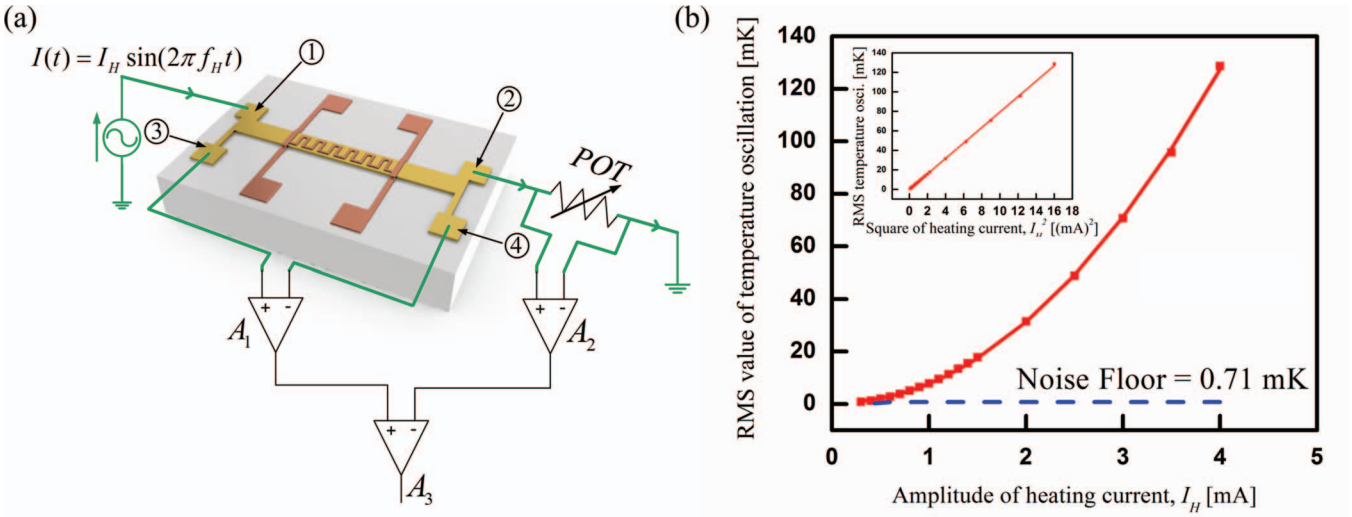

FIG. 5. Characterization of the relationship between the RMS value of temperature oscillations and the amplitude of the heating current. (a) Schematic diagram of the measurement configuration used to measure the RMS values of temperature oscillations of the heater line. A potentiometer is placed in series to implement a differential scheme that enables the isolation of the $3f_H$ component of the voltage signal. (b) Measured RMS values of the temperature oscillation of the bottom heater line as a function of the amplitude of the heating electrical current. The frequency of the heating current is chosen to be 20 Hz. Inset shows the same data plotted as a function of square of the amplitude of the heating current, the relationship is linear as expected (the R-square measure of goodness of fit is 0.999).

10. The voltage output of these two amplifiers was supplied to another instrumentation amplifier (A3, Analog Devices -AD524), which was operated at unity gain. This enabled us to subtract the voltage component at a frequency f_H. The voltage output of this instrumentation amplifier was supplied to a lock-in amplifier (SRS-SR830) to measure the RMS value of voltage oscillations at $3f_H$. Finally, the RMS value of the temperature oscillations is related to the RMS value of the voltage oscillations. The measured RMS values of temperature oscillations for various amplitudes of sinusoidal electrical currents ($f_H = 20$ Hz,) are shown in Fig. 5(b). The measured temperature oscillation is also plotted as a function of I_H^2 in Fig. 5(b) inset. Indeed, we find that the measured temperature oscillations increase linearly with I_H^2.

A. Noise floor of the 3*f*-technique

The 3*f*-measurement technique described above uses the same electrical current to both induce a temperature oscillation via heating as well as for sensing the temperature oscillations. This implies that when the amplitude of temperature oscillations is small, the amplitude of the heating (sensing) electric current is also low. This lack of independent control on the sensing and heating currents limits the ability to measure temperature oscillations of small amplitudes because the voltage output at $3f_H$ is directly proportional to the amplitude of the sensing current. Hence, the noise floor in the measurement of temperature oscillations is relatively high. For example, the noise floor in our measurements is ~1 mK and is shown by the dashed line in Figure 5(b).

B. Measurement of temperature oscillations with the platinum resistance thermometer

In order to independently measure the temperature oscillations in the PRT resistor resulting from the heating of the bottom heater, we adopted the measurement configuration shown in Fig. 6. A dc current, $I_{DC} = 10\ \mu$A, generated using a custom built current source (see Fig. 6 inset) was supplied through the PRT. In addition to a dc component, the voltage across the probe electrodes (3, 4 in Fig. 6) also has a component at $2f_H$, arising from the interaction of the dc current and the temperature-dependent electrical resistance. In fact, the RMS value of the sinusoidal temperature oscillation of the PRT (ΔT_{2f_H}) can be related to the RMS value of the voltage oscillation V_{2f_H} by $\Delta T_{2f_H} = V_{2f_H}/[I_{DC} R\alpha]$.

In order to isolate the signal of interest (V_{2f_H}) from the large dc voltage across the resistor, we placed an identical thin film resistor (matching resistor) in series with the PRT (Fig. 6), which was also located inside the cryostat. Thus both resistors experience nearly identical ambient temperature and thermal drifts. Further, a potentiometer was used in series with the thin-film resistors (located outside the cryostat) to trim the dc voltage across the PRT and matching resistor to be equal (see Fig. 6). The voltage signals across the PRT and across the matching thin film resistor and the potentiometer are measured with two precision instrumentation amplifiers (A4, A5, Analog Devices-AD524) operated at a gain of 100. The differential temperature signal from these outputs was obtained using a second stage monolithic low noise amplifier (A6) with a wideband, low distortion and high common mode rejection ratio (Burr-Brown-INA103). Finally, the voltage output of this instrumentation amplifier was supplied to a lock-in amplifier (SRS-SR830) to measure the RMS value of the voltage oscillations at $2f_H$. The measured RMS values were used to obtain the RMS values of the temperature oscillations. Figure 7 shows the measured RMS values of temperature oscillations of the PRT line along with the measured RMS values of the heater line for various frequencies and amplitudes of temperature oscillations. The data suggest that the RMS values of the temperature oscillations in the bottom and top heaters are identical for the entire range of heating currents—demonstrating that the PRT and the heater lines

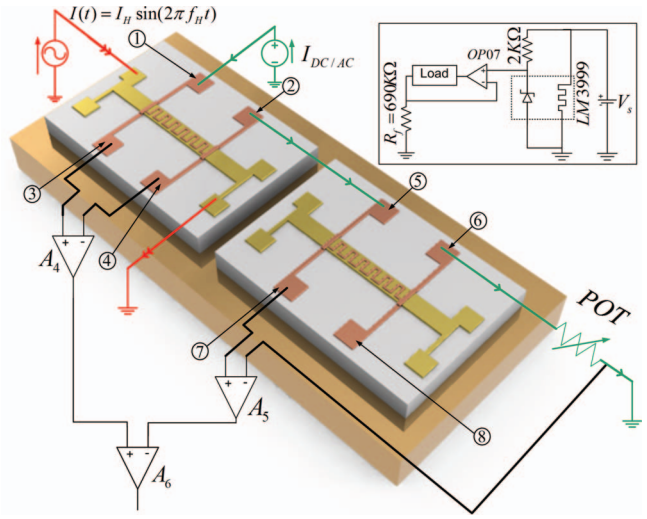

FIG. 6. Schematic diagram of the instrumentation setup used to measure the amplitude of temperature oscillations of the PRT. A differential measurement scheme is used to reject the noise arising from the non-ideality of the current source and to eliminate the effects of thermal drift. Inset: schematic diagram of the custom-built current source.

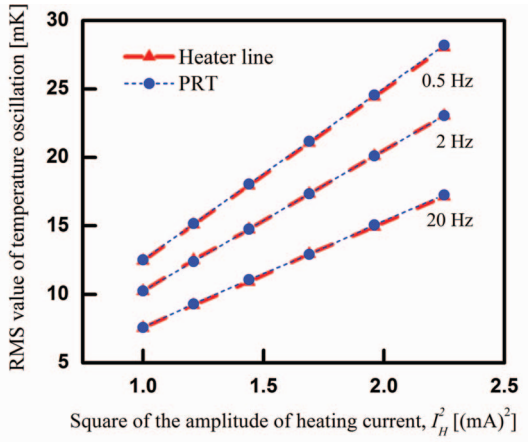

FIG. 7. Characterization of the thermal contact between the heater line and the PRT. The measured RMS values of the temperature oscillations of the heater and the PRT, due to a sinusoidal thermal excitation of the heater line. The RMS values increase linearly with the magnitude of the square of the amplitude of the heating current. Further, the bottom and top line temperatures are identical. This provides strong support for the conclusion that the heater and PRT are in excellent thermal contact. The measurements were performed over a range of heating frequencies ($2f_H = 0.5$ Hz, 2 Hz, and 20 Hz).

are in excellent thermal contact. We note that increasing frequencies of heating current lead to progressively smaller temperature oscillations, such dependence on frequency is indeed expected and well understood from basic heat transfer theory.[18]

Finally, we emphasize that all the measurements of the temperature oscillations shown in Fig. 7 were performed for a range of heating currents that produce temperature oscillations that are above the noise floor of the 3*f* technique, so as to enable a direct measurement of the temperature oscillations of both the heater and the PRT.

V. POWER SPECTRAL DENSITY OF NOISE

In order to enable an estimation the NET of each of the schemes described above it is necessary to experimentally determine $PSD_{Amp\ Total,\ RTI}$ and $PSD_{\Delta T,\ Drift}$. In this section, we present our experimentally measured data of these power spectral densities. Further, we also provide the estimated temperature resolution for each of the schemes described above.

A. Characterization of power spectral densities ($PSD_{Amp\ Total,\ RTI}$ and $PSD_{\Delta T,\ Drift}$)

The general strategy used in this work to obtain the desired power spectral densities is as follows. We begin by configuring a setup represented by the schematic shown in Fig. 8. First, an unmodulated current $Is = I_{DC}$, from a custom-built current source (Fig. 6 inset), is supplied through the PRT of the microdevice and a matching resistor (identical resistance thin film device and potentiometer, see Fig. 8) while the heating current was turned off. The voltage output of the second stage amplifier, which measures the differential voltage between the voltage drop across the microdevice and the voltage drop across the matching resistor was monitored to characterize the noise. It is to be expected that the voltage noise has contributions from various noise sources including shot noise and temperature drift. The contributions of various noise sources to the power spectral density of the voltage noise at the output ($PSD_{with\ I_s=I_{DC}}$) can be estimated using Eq. (5), for any given magnitude of the sensing current. When the supplied current I_s is turned off, the resultant power spectral density ($PSD_{with\ I_s=0\ Amp}$) is smaller, at all frequencies, as the contributions from shot noise and temperature drift are eliminated. We note that $PSD_{with\ I_s=I_{DC}}$ can be related to $PSD_{Amp\ Total}$ (see Eq. (5)) and $PSD_{\Delta T,\ Drift}(f)$ by $PSD_{with\ I_S=I_{DC}}(f) = PSD_{Amp\ total} + [(I_{DC}R\alpha)^2\ PSD_{\Delta T,\ Drift}(f)]G_1^2G_2^2$. Using this equation and Eqs. (2) and (5), it can be shown that

$$PSD_{with\ I_S=I_{DC}}(f) - PSD_{with\ I_S=0Amp}(f) = [(I_{DC}R\alpha)^2\ PSD_{\Delta T,\ Drift}(f) + 2PSD_{I=I_{DC},\ Shot}(f)R^2]G_1^2G_2^2. \quad (25)$$

This suggests that by measuring the power spectral densities of voltage output with and without a current, it is possible to experimentally obtain a linear combination of the power spectral densities of temperature drift and shot noise (RHS of Eq. (25)). We also note that the power spectral density of temperature drift ($PSD_{\Delta T,\ Drift}(f)$) at high frequencies (>500 Hz) is negligible, as the temperature cannot fluctuate significantly at high frequencies due to thermal inertia. Thus, at high frequencies, the right hand side of Eq. (25) consists primarily of contributions from shot noise, hence $PSD_{I=I_{DC},Shot}(f)$ can be easily obtained at high frequencies. Further, since $PSD_{I=I_{DC},Shot}(f)$ is expected to be relatively independent of frequency, the obtained high frequency $PSD_{I=I_{DC},Shot}$ is representative of the shot noise at all frequencies. The discussion above highlights the fact that $PSD_{\Delta T,\ Drift}(f)$ can be experimentally determined by measuring $PSD_{with\ I_s=I_{DC}}$ and $PSD_{with\ I_s=0\ Amp}$. Finally, ($PSD_{Amp\ Total,\ RTI}$) can also be obtained by adding the contribution of shot noise to $PSD_{with\ I_s=0\ Amp}$. Specifically, ($PSD_{Amp\ Total,\ RTI}$) is given by

$$PSD_{Amp\ Total,RTI}(f) = [(PSD_{with,\ I_s=0}(f))/(G_1G_2)^2] + [2PSD_{I=I_{DC},Shot}(f)R^2]. \quad (26)$$

In order to experimentally determine $PSD_{with\ I_s=I_{DC}}$ and $PSD_{with\ I_s=0\ Amp}$ we used the configuration shown in Fig. 8. In this experiment, we first applied a dc sensing current of 10 μA to the PRT, which was found to be adequate for estimating the desired power spectral densities. The voltage output of the second stage amplifier (Fig. 8) was simultaneously monitored to obtain the power spectral density using a commercial FFT analyzer (SR 770, Stanford Research Systems). Precautions were taken to eliminate extraneous sources of noise by carefully shielding all the wires and the devices from stray electromagnetic fields: the cryostat chamber used in the experiment was grounded and the low level, differential signals were collected with cables employing individually shielded and twisted pairs. Further, special care was taken to avoid ground loops.[19]

Figure 9(a) shows the measured power spectral densities (at 280 K) of $PSD_{with\ I_s=I_{DC}}$ and $PSD_{with\ I_s=0\ Amp}$ relative to the inputs (i.e., measured power spectral density divided by $G_1^2G_2^2$). As expected, $PSD_{with\ I_s=I_{DC}}$ is greater

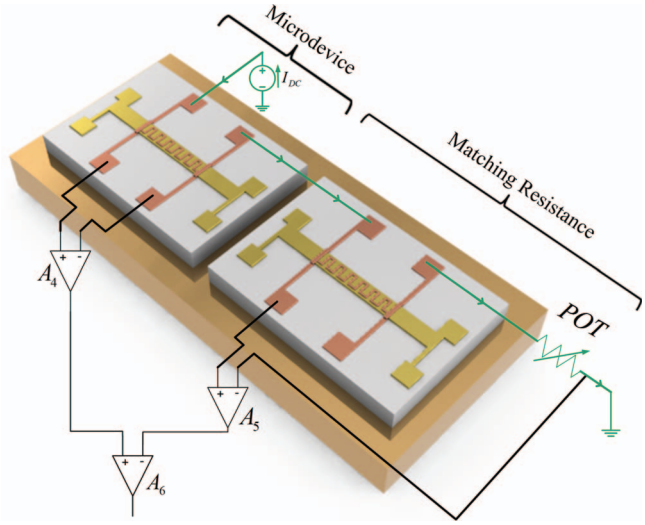

FIG. 8. Schematic diagram of the measurement setup used to obtain the power spectral densities $PSD_{Amp\ Total,\ RTI}$ and $PSD_{\Delta T,\ Drift}$. These PSDs are required to estimate the NET of the four schemes described in this study.

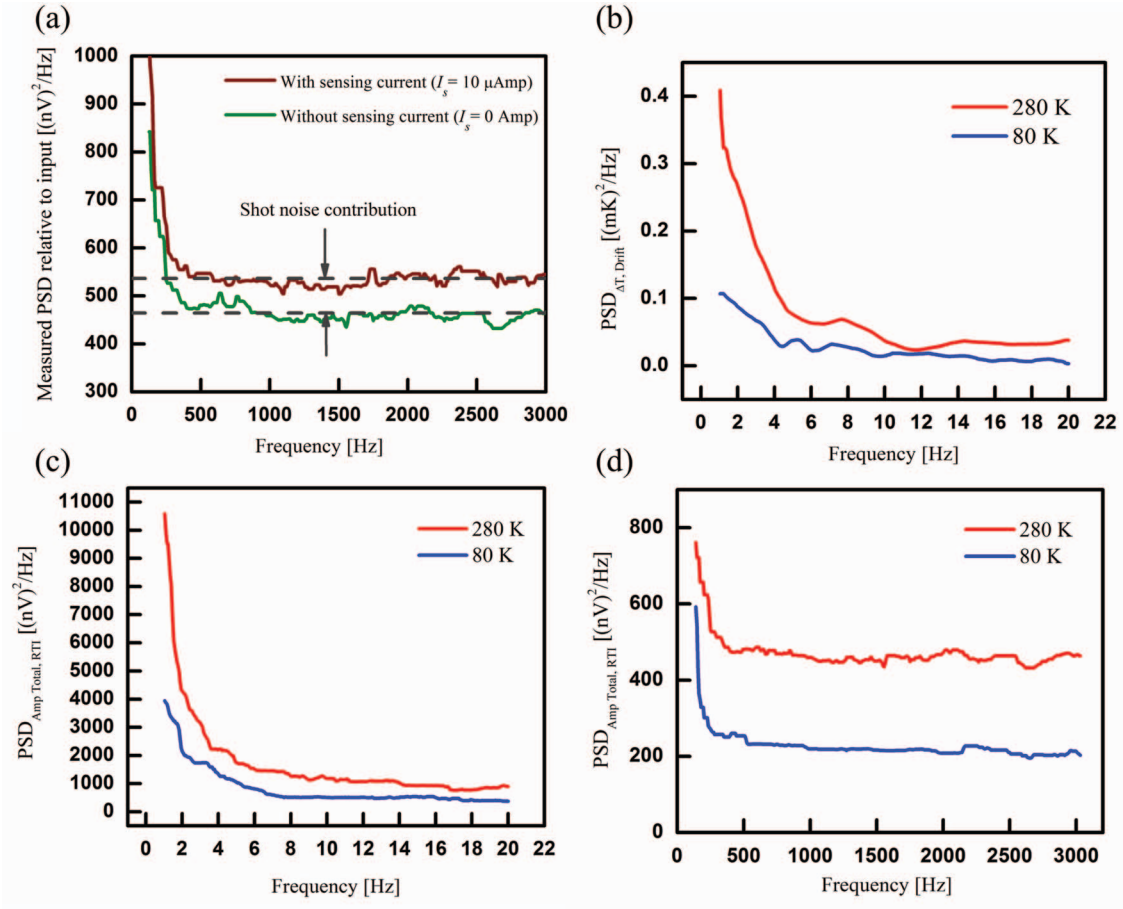

FIG. 9. Experimental determination of $PSD_{Amp\ Total,\ RTI}$ and $PSD_{\Delta T,\ Drift}$. Panel (a) shows the measured power spectral densities (at 280 K) of $PSD_{with\ I_s=I_{DC}}$ and $PSD_{with\ I_s=0\ Amp}$ relative to the inputs (i.e., measured power spectral density divided by $G_1^2G_2^2$). The larger power spectral density of $PSD_{with\ I_s=I_{DC}}$, at high-frequencies, is attributed to shot noise as discussed in the text. The shot noise contribution is seen to be relatively independent of the frequency (b) $PSD_{\Delta T,\ Drift}$ for a range of frequencies (1–20 Hz), at two different temperatures (80 K, 280 K) was obtained by first measuring $PSD_{with\ I_s=I_{DC}}$ and $PSD_{with\ I_s=0\ Amp}$ in the frequency range of interest and using Eq. (25) described in the text. (c) Measured $PSD_{Amp\ Total,\ RTI}$ of thermometer at 80 K and 280 K in a range of frequencies (1–20 Hz), and (d) measured $PSD_{Amp\ Total,\ RTI}$ of thermometer at 80 K and 280 K in a larger range of frequencies (1 Hz–3 kHz). The data presented in the figure were obtained by first averaging the measured PSD in 200 individual experiments ((a) and (d)) and 20 individual experiments ((b) and (c)) and subsequently performing further averaging using a 20 point median averaging scheme.

than $PSD_{with\ I_s=0\ Amp}$ at high frequencies (500 Hz–3 KHz), and the difference is relatively invariant with frequency. The measured difference suggests that $2PSD_{I=I_{DC,Shot}}(f)\cdot R^2$ is ~75 nV^2/Hz, in the range from 500 Hz to 3 KHz, which is much smaller than the power spectral density estimated from the equation for shot noise described earlier (estimated shot noise equals $2(2eI_SR^2) \sim 6400nV^2$/Hz). We note that this smaller shot noise value is to be expected because the custom-built current source (Fig. 6 inset) used in our experiments employs negative feedback which is well known to suppress shot noise.[20] Further, the long range electronic correlations in metallic conductors are also known to suppress shot noise.[20] Using the measured power spectral density of shot noise in conjunction with Eq. (25), we obtained the ($PSD_{\Delta T,\ Drift}$) at 280 K which is shown in Fig. 9(b) for the frequency ranges 1–20 Hz. Following a similar procedure, we also obtained ($PSD_{\Delta T,\ Drift}$) at 80 K, which is also shown in Fig. 9(b). It can be seen that the low-frequency part of the spectrum is dominated by *1/f* noise, while the high-frequency part of the spectrum shows broadband noise that is relatively independent of frequency. In addition to this, we also obtained ($PSD_{Amp\ Total,\ RTI}$) using the measured data and Eq. (26). The obtained power spectral densities are shown in Fig. 9(c) (1 Hz–20 Hz) and 9d (1 Hz–3 KHz) for a range of frequencies. These data were obtained by first averaging the measured PSD from 200 individual experiments for Figs. 9(a) and 9(d) and 20 individual experiments for Figs. 9(b) and 9(c) and subsequently performed twenty point median averaging to obtain smooth spectral density estimates.

Finally, to estimate the NETs in scheme 1 and 2, as well as for estimating NETs for low frequency temperature modulations (0.5 Hz) in scheme 3 and 4, it is necessary to know the values of $PSD_{\Delta T,\ Drift}$ in a range of frequencies close to 0 Hz. Therefore, we obtained $PSD_{with\ I_S=I_{DC}}(f)$ and $PSD_{with\ I_S=0Amp}(f)$ in a narrow band of $f = 0$ to 1 Hz in frequency intervals of $\Delta f = 0.477$ mHz (Fig. 10(a)). The obtained power spectral densities of $PSD_{Amp\ Total,\ RTI}$ and $PSD_{\Delta T,\ Drift}$ are shown in Figs. 10(b) and 10(c), respectively. The curves shown in Fig. 10(a) were obtained by averaging five individual spectral density estimates and by curve-fitting a ninth order polynomial function to the data. Further, 95% confidence intervals of the curve fits were determined

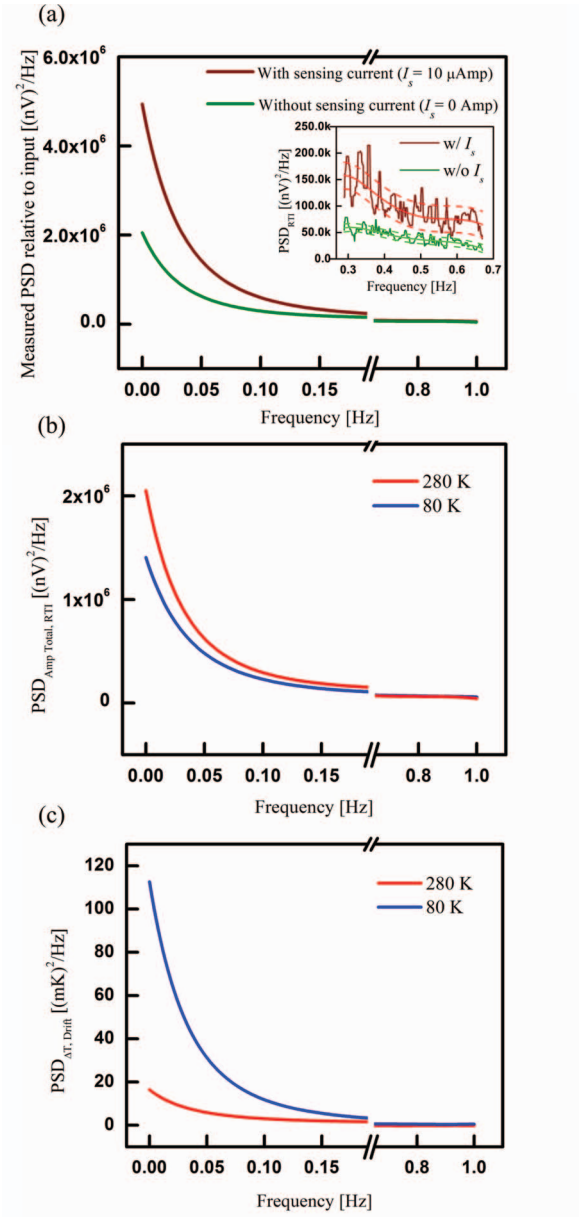

FIG. 10. Measurement of amplifier noise and temperature drift at low frequencies. We determined the $PSD_{Amp\ Total,\ RTI}$ (b) and $PSD_{\Delta T,\ Drift}$ (c) in the narrow frequency range of 0 to 1 Hz from the $PSD_{with\ I_S=I_{DC}}(f)$ and $PSD_{with\ I_S=0Amp}(f)$ shown in (a) by averaging five individual curves and by curve fitting the averaged data. The data shown in panels (b) and (c) were obtained by using the data presented in panel (a). As a representative example, the inset (a) shows the measured PSD at 0.5 Hz along with the curve fits and the corresponding 95% confidence intervals.

to estimate the uncertainty in the measured PSD (see inset Fig. 10(a)). The PSD of the total amplifier noise and temperature drift were obtained by using the data presented in Fig. 10(a) and are shown in Figs. 10(b) and 10(c). Both the estimates shown in Figs. 10(b) and 10(c) have a small uncertainty (not shown in the figure) that arises from the uncertainty in the fits to the data presented in Fig. 10(a).

B. Estimated NET for the thermometry schemes

The measured PSDs enable an estimate of the NET for each of the schemes described above by using the expressions provided in Sec. III. For all the estimates provided below we arbitrarily assume a measurement bandwidth of ∼16 mHz. Further, we assume that the sensing current used in all the experiments is either a dc current of 10 μA or an ac current with an amplitude of 10 μA. This choice of the magnitude of the current corresponds well to currents used in suspended-microscale devices that are employed for probing nanoscale heat transfer.[1] We note that the chosen magnitude represents a tradeoff between choosing a large magnitude of current to improve the signal to noise ratio while keeping the current small to avoid self-heating effects in suspended devices.

TABLE II. The estimated resolution of the four different schemes of resistance thermometry. The resistance of the PRT is assumed to be 10 kΩ while the bandwidth of measurement is set to 16 mHz.

	Global temperature (K)	Thermometry resolution (μK)		
Scheme 1	280	2463 ± 316		
$f_s = 0$	80	1573 ± 172		
$f_T = 0$				
Scheme 2		$f_s = 20$ Hz	$f_s = 500$ Hz	$f_s = 1000$ Hz
$f_s \neq 0$	280	702 ± 15	702 ± 15	702 ± 15
$f_T = 0$	80	271 ± 14	270 ± 14	270 ± 14
Scheme 3		$f_T = 0.5$ Hz	$f_T = 2$ Hz	$f_T = 20$ Hz
$f_s = 0$	280	212 ± 31	78 ± 21	34 ± 17
$f_T \neq 0$	80	181 ± 11	53 ± 20	27 ± 18
Scheme 4		$f_T = 0.5$ Hz	$f_T = 2$ Hz	$f_T = 20$ Hz
$f_s = 500$ Hz	280	81 ± 43	48 ± 12	30 ± 8
$f_T \neq 0$	80	43 ± 27	32 ± 12	23 ± 9

Table II lists the calculated NETs for the four schemes along with the uncertainty in the NETs estimated using the curve fits and confidence intervals to the measured data. These NETs were computed at two different temperatures (80 K and 280 K) by using Eqs. (10), (14), (19), and (24) and the data presented in Figs. 9 and 10. As expected, it can be seen that the NET for scheme 1 is relatively large, ∼1.5 mK even at low temperatures. This large NET is associated with the large values of $PSD_{Amp\ Total,\ RTI}$ and $PSD_{\Delta T,\ Drift}$ at low frequencies. For scheme 2, the NET is found to be ∼0.7 mK at 280 K and ∼0.3 mK at 80 K and is relatively independent of the sensing frequency. This lack of dependence on sensing frequency—in this case—can be understood by noting that the NET has large contributions from $PSD_{\Delta T,\ Drift}$ which is independent of the sensing frequency (20 Hz, 500 Hz, 1000 Hz) as can be seen from Eqs. (13) and (14). This NET can potentially be improved if the sensing and matching resistors are integrated into a substrate with a high thermal conductivity. For comparison, Wingert *et al.*[2,8] have recently shown that for samples made on a silicon substrate, with a thermal conductivity ∼100 times larger than that of the glass substrates used in this study, it was possible to achieve a resolution of ∼0.6 mK in a bandwidth of ∼260 mHz (as opposed to the ∼16 mHz bandwidth used in this study). This improved resolution can potentially be attributed to smaller $PSD_{\Delta T,\ Drift}$ in their devices. However, it is not always possible to use such highly thermally conducting substrates, therefore, it is important to quantify the effect of $PSD_{\Delta T,\ Drift}$. Additional improvements in the NET could

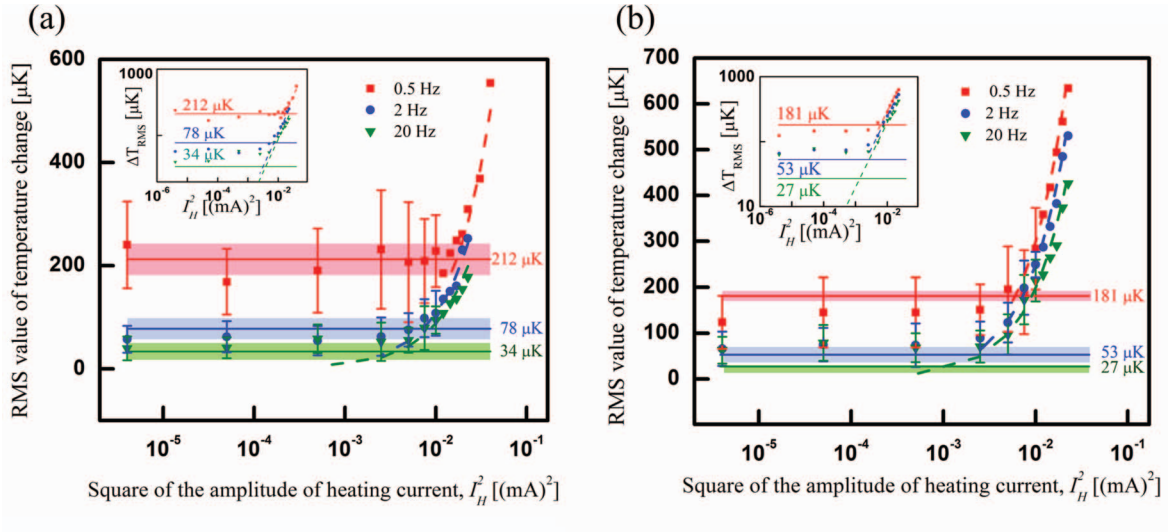

FIG. 11. Experimental demonstration of the resolution of scheme 3. In this scheme modulated temperature changes are detected using an unmodulated sensing current. Part (a) shows the measured RMS values of the temperature oscillations of the PRT, at an ambient temperature of 280 K, when the heater line is excited using sinusoidal heating currents (0.5, 2.0, and 20 Hz). The dashed lines in the figure represent the expected RMS temperature values based on data shown in Fig. 7. The error bars above reflect the standard deviation in the RMS value reported by the lock-in amplifier. The solid lines show the estimated noise floor for NET measurements performed at each of the frequencies, while the bands represent the uncertainty of the NET estimates. The inset presents the same data in a log-log plot. Figure (b) shows data otherwise identical to those in (a) for measurements performed at 80 K.

potentially be obtained, for both scheme 1 and 2, by carefully attenuating the temperature drift of the electronics to small values (∼mK): this would enable a reduction in the low frequency voltage noise.

For scheme 3, where the temperature changes to be measured are modulated, the NET is found to be substantially smaller (<100 μK) for large modulation frequencies (2 Hz, 20 Hz). This improvement in NET arises primarily from a reduction in both $PSD_{Amp\ Total,\ RTI}$, and $PSD_{\Delta T,\ Drift}$ at high frequencies. Finally, for scheme 4, we estimated the resolution for a sensing current frequency of 500 Hz and for various temperature modulation frequencies. It can be seen that, as expected, at low modulation frequencies the NET can be improved by approximately a factor of three in comparison to scheme 3. On the other hand, at higher frequencies (2 Hz, 20 Hz) the estimated NET of scheme 4 is comparable to that of scheme 3.

A final question to be addressed is if the predicted NETs can actually be achieved with a commercial lock-in amplifier (SRS-SR830) which enables convenient, continuous monitoring of temperature signals. To answer this question we experimentally implemented schemes 3 and 4. We focused on these schemes because of their superior resolution and the fact that a variation of scheme 2 has been recently discussed in the literature.[2,8]

VI. EXPERIMENTAL VERIFICATION OF THE NET FOR SCHEMES 3 AND 4

In order to experimentally measure the NET of the PRT in schemes 3 and 4 we supplied sinusoidal electrical currents with relatively small amplitudes to the Au heater line, which resulted in temperature oscillations of the PRT with small RMS values. We note that based on the data shown in Fig. 7 (data obtained at 280 K) and similar data obtained at 80 K it is possible to estimate the expected RMS values of temperature oscillations for currents of small amplitudes. In fact, the dashed lines in Figs. 11 and 12 show estimated temperature raises at 280 K and 80 K, for sinusoidal excitation by currents of small amplitudes at various frequencies. We now describe the experiments performed by us to experimentally establish the resolution of schemes 3 and 4.

A. Measured RMS values of temperature modulations in scheme 3

Temperature oscillations of the PRT, resulting from sinusoidal heating currents of small amplitudes, were measured by supplying a dc sensing current ($I_{DC} = 10^{-5}$ amp) and monitoring the $2f_H$ component of the voltage (V_{2f_H}) using a commercial lock-in amplifier, in a bandwidth of ∼16 mHz, following the configuration shown in Fig. 6. The RMS values of the resultant temperature oscillations (ΔT_{2f_H}), arising from heating currents of varying amplitudes and frequencies (0.5 Hz, 2 Hz, and 20 Hz), were obtained from the measured voltage oscillations using the relationship $\Delta T_{2f_H} = V_{2f_H}/(I_{DC} R\alpha)$ and are shown in Fig. 11(a). Further, the expected values of temperature oscillations from the data shown in Fig. 7 are also plotted (dashed lines) along with the expected NETs and their corresponding uncertainties (from Table II), which are represented by solid lines and solid bands, respectively. It can be seen that the measured temperature oscillations are in good agreement with the expected values (dashed lines). Further, it can also be seen that the smallest temperature that could be measured is in good agreement with the expected NET values. Figure 11(b) shows otherwise identical data obtained at a temperature of 80 K. Again, it can be seen that the smallest temperature that could be resolved at various frequencies is in good agreement with estimated values of NET. Experiments performed at other temperatures (130 K,

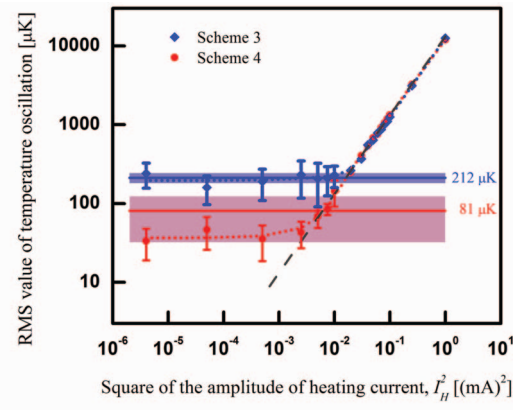

FIG. 12. Experimental demonstration of the resolution of scheme 4 at low modulation frequencies (0.5 Hz). Modulated temperature changes were measured using a modulated sensing current at 500 Hz. All measurements were performed at 280 K. The dashed line represents the expected temperature RMS values based on the data shown in Fig. 7. The dotted lines show curve fits to the measured data. The error bars above reflect the standard deviation in the RMS value reported by the lock-in amplifier. The solid lines and bands show the estimated NETs and the uncertainty in the estimated NETs, respectively.

180 K, 230 K) are also found to be in good agreement with estimated NETs and are not presented here in the interest of space. Finally, we note that, as expected, the NET at low frequencies (0.5 Hz) is significantly larger than that at high frequencies due to contributions from *1/f* voltage noise. Next, we show that the temperature resolution of low frequency measurements can be improved substantially using a modulated sensing current.

B. Measured RMS values of temperature modulations in scheme 4

We performed an experiment (at 280 K) where temperature oscillations of the PRT at f_T (0.5 Hz) were measured using an ac sensing current with an amplitude $I_{AC} = 10^{-5}$ amp and a sensing frequency $f_S = 500$ Hz. The measurement configuration used for accomplishing this goal is shown in Fig. 6. As described in Sec. IV, the voltage output of the second stage amplifier has information regarding the temperature oscillation of the PRT at two frequencies: $f_S + f_T$ and $f_S - f_T$. In order to extract these signals, we monitored the voltage output of the second stage amplifier using two lock-in amplifiers, set to a bandwidth of ~16 mHz, to independently measure the components of the signal at $f_S + f_T$ and $f_S - f_T$. In order to provide the appropriate reference signal to the lock-in amplifiers we used four function generators (Agilent 33521A) that were synchronized using a master clock. Two of these function generators in conjunction with the custom built current source (a modified version of the circuit shown in the inset of Fig. 6) were used to generate the desired heating and sensing sinusoidal currents at the appropriate frequencies, f_T and f_S, respectively. The remaining two function generators provided the reference signals required by the lock-in amplifiers to extract the voltage signals of interest at $f_S - f_T$ and $f_S + f_T$. The RMS values of the voltages measured by two lock-in amplifiers ($V_{f_S+f_T}$, $V_{f_S-f_T}$) were added to obtain the resultant voltage $V_R = V_{f_S+f_T} + V_{f_S-f_T}$. Finally, the RMS value of the temperature oscillation of the PRT was obtained from $\Delta T_{RMS,f_T} = V_R/[I_{AC} R\alpha]$.

The measured amplitude of temperature oscillations using scheme 4, at 280 K, for a range of heating currents are shown in Fig. 12. Further, the results obtained for the same heating currents using scheme 3 are also shown for comparison. It can be clearly seen—as predicted by our analysis—that the temperature resolution of scheme 4 (~40 μK) is much better than the temperature resolution of scheme 3 (~250 μK). The measured NET is also in good agreement with the predicted values, which are shown as a band to represent the uncertainty in the predicted NETs (Table II). Similar experiments performed at 80 K also show good agreement with the estimated NETs and not shown here in the interest of space.

VII. CONCLUSION

We have presented a broad analysis of the different scenarios of electrical resistance-based thermometry that are suitable for nanoscale heat transport studies. Our detailed analysis delineates the contributions of both the voltage noise resulting from intrinsic and extrinsic sources and the voltage noise arising from temperature drift. Further, our analysis quantifies the noise equivalent temperature that is in principle achievable using different thermometry schemes. Our experiments and analysis demonstrate that it is beneficial to use a scheme where the temperature can be modulated as this enables the measurement of temperature changes with high resolution due to its immunity to low temperature drift. Our work also points out that if the temperature cannot be modulated, high resolution thermometry can still be accomplished by using a modulated sensing current and a matching thin film resistor which has a temperature drift that corresponds to that of the sensing resistor. Finally, our work shows that it is readily possible to resolve temperature changes with electrical resistance-based thermometry well below 100 μK which we believe will enable a dramatic improvement in the heat-current resolution of microdevices used for probing nanoscale phonon and photon transport.

ACKNOWLEDGMENTS

This work is pursued as part of the Center for Solar and Thermal Energy Conversion, an Energy Frontier Research Center funded by the US Department of Energy, Office of Science, Office of Basic Energy Sciences under Award No. DE-SC0000957.

APPENDIX: ESTIMATE OF THE POWER SPECTRAL DENSITY OF TEMPERATURE DRIFT-RELATED VOLTAGE NOISE IN SCHEMES 2 AND 4

When a sinusoidal sensing current is used the voltage noise associated with temperature drift ($\Delta T(t) = \Delta T_{drift}$) is given by

$$V_{temperature\,drift}(t) = V(t) = (I_S R\alpha) sin(2\pi f_S t) \cdot \Delta T(t), \quad \text{(A1)}$$

which can be represented as the sum of the two signals:

$$V(t) = \underbrace{\left(\frac{I_s R\alpha}{2i}\right) e^{i2\pi f_s t} \cdot \Delta T(t)}_{y_1(t)} + \underbrace{\left(-\frac{I_s R\alpha}{2i}\right) e^{-i2\pi f_s t} \cdot \Delta T(t)}_{y_2(t)}. \tag{A2}$$

The power spectral density of $V(t)$, $PSD_V(f)$ can be related to the autocorrelation function of $V(t)$. The autocorrelation function $R_{VV}(\tau)$ is given by

$$\begin{aligned} R_{VV}(\tau) &= \langle V^*(t)V(t+\tau)\rangle \\ &= \lim_{T\to\infty} \frac{1}{T}\int_{-T}^{+T} V^*(t)V(t+\tau)dt, \end{aligned} \tag{A3}$$

and is related to the one-sided power spectral density by

$$PSD_V(f) = G_V(f) = \int_{-\infty}^{+\infty} 2R_{VV}(t)e^{-i2\pi ft}dt. \tag{A4}$$

From Eq. (A2)

$$R_{VV}(\tau) = \langle [y_1^*(t) + y_2^*(t)] \times [y_1(t+\tau) + y_2(t+\tau)]\rangle, \tag{A5}$$

this implies that

$$R_{VV}(\tau) = R_{y_1y_1}(\tau) + R_{y_2y_2}(\tau) + R_{y_1y_2}(\tau) + R_{y_2y_1}(\tau), \tag{A6}$$

where $R_{y_1y_2}(\tau)$ and $R_{y_2y_1}(\tau)$ are the cross-correlation functions between $y_I(t)$ and $y_I(t)$. Using Eqs. (A2)–(A4) and (A6) it can be show that

$$\begin{aligned} G_V(f) = \frac{(I_s R\alpha)^2}{4}\Bigg[& G_{\Delta T}(f-f_s) + G_{\Delta T}(f+f_s) \\ & - \lim_{T\to\infty}\frac{2}{T}[\Delta T^*(f-f_s)\Delta T(f+f_s)] \\ & + \Delta T^*(f+f_s)\Delta T(f-f_s)\Bigg], \end{aligned} \tag{A7}$$

where $G_{\Delta T} = PSD_{\Delta T,\,Drift}$ is the power spectral density of temperature drift as defined in Sec. II and $\Delta T(f)$ represents the Fourier components of the temperature drift signal. When $(f - f_s) \to 0$, $PSD_{\Delta T,\,Drift}(f - f_S)$ dominates over all other terms suggesting that when $f \to f_s$,

$$PSD_V(f) = G_V(f) \sim \frac{(I_s R\alpha)^2}{4} PSD_{\Delta T,Drift}(f - f_s), \tag{A8}$$

which can be used to obtain Eq. (13) of the article. Similarly, Eq. (23) of the manuscript can also be obtained using Eq. (A7) and the approximations described above.

[1] L. Shi, D. Y. Li, C. H. Yu, W. Y. Jang, D. Y. Kim, Z. Yao, P. Kim, and A. Majumdar, J. Heat Transfer **125**(6), 1209 (2003).
[2] M. C. Wingert, Z. C. Y. Chen, E. Dechaumphai, J. Moon, J. H. Kim, J. Xiang, and R. K. Chen, Nano Lett. **11**(12), 5507 (2011).
[3] S. Shen, A. Henry, J. Tong, R. T. Zheng, and G. Chen, Nat. Nanotechnol. **5**(4), 251 (2010).
[4] K. Schwab, E. A. Henriksen, J. M. Worlock, and M. L. Roukes, Nature (London) **404**(6781), 974 (2000).
[5] S. Sadat, Y. J. Chua, W. Lee, Y. Ganjeh, K. Kurabayashi, E. Meyhofer, and P. Reddy, Appl. Phys. Lett. **99**(4), 043106 (2011).
[6] O. Bourgeois, S. E. Skipetrov, F. Ong, and J. Chaussy, Phys. Rev. Lett. **94**(5), 069904 (2005); W. C. Fon, K. C. Schwab, J. M. Worlock, and M. L. Roukes, Nano Lett. **5**(10), 1968 (2005); A. F. Lopeandia, L. I. Cerdo, M. T. Clavaguera-Mora, L. R. Arana, K. F. Jensen, F. J. Munoz, and J. Rodriguez-Viejo, Rev. Sci. Instrum. **76**(6), 065104 (2005); B. L. Zink, R. Pietri, and F. Hellman, Phys. Rev. Lett. **96**(5), 055902 (2006).
[7] K. Kim, W. Jeong, W. Lee, and P. Reddy, ACS Nano **6**(5), 4248 (2012); L. Shi, S. Plyasunov, A. Bachtold, P. L. McEuen, and A. Majumdar, Appl. Phys. Lett. **77**(26), 4295 (2000).
[8] M. C. Wingert, Z. C. Y. Chen, S. Kwon, J. Xiang, and R. K. Chen, Rev. Sci. Instrum. **83**(2), 024901 (2012).
[9] A. Sikora, H. Ftouni, J. Richard, C. Hebert, D. Eon, F. Omnes, and O. Bourgeois, Rev. Sci. Instrum. **83**(5), 054902 (2012).
[10] S. Shen, A. Narayanaswamy, and G. Chen, Nano Lett. **9**(8), 2909 (2009); J. R. Barnes, R. J. Stephenson, M. E. Welland, C. Gerber, and J. K. Gimzewski, Nature (London) **372**(6501), 79 (1994).
[11] J. Varesi, J. Lai, T. Perazzo, Z. Shi, and A. Majumdar, Appl. Phys. Lett. **71**(3), 306 (1997).
[12] B. W. Mangum, J. Res. Natl. Bur. Stand. **89**(4), 305 (1984).
[13] P. R. N. Childs, in *Advances in Heat Transfer*, edited by T. F. Irvine, Y. I. Cho, J. P. Hartnett, and A. G. George (Elsevier, 2003), Vol. 36, p. 111; P. R. N. Childs, J. R. Greenwood, and C. A. Long, Rev. Sci. Instrum. **71**(8), 2959 (2000).
[14] J. M. Ziman, *Electrons and Phonons : The theory of Transport Phenomena in Solids* (Oxford University Press, New York, 2001).
[15] C. V. Heer, *Statistical Mechanics, Kinetic Theory, and Stochastic Processes* (Academic, New York, 1972).
[16] B. Razavi, *Design of Analog CMOS Integrated Circuits* (McGraw-Hill, Boston, MA, 2001).
[17] A. Papoulis and S. Unnikrishna Pillai, *Probability, Random Variables, and Stochastic Processes*, 4th ed. (McGraw-Hill, Boston, 2002).
[18] H. S. Carslaw and J. C. Jaeger, *Conduction of Heat in Solids*, 2nd ed. (Oxford University Press, New York, 1986).
[19] H. W. Ott, *Noise Reduction Techniques in Electronic Systems*, 2nd ed. (Wiley, New York, 1988).
[20] P. Horowitz and W. Hill, *The Art of Electronics*, 2nd ed. (Cambridge University Press, Cambridge, England; New York, 1989).